



**HAL**  
open science

# Low-cost non-intrusive sensitivity analysis technique for heat and mass transfer in porous media, with application to space-vehicle heat-shield design

Mickael Rivier, Jean Lachaud, Pietro Marco Congedo

## ► To cite this version:

Mickael Rivier, Jean Lachaud, Pietro Marco Congedo. Low-cost non-intrusive sensitivity analysis technique for heat and mass transfer in porous media, with application to space-vehicle heat-shield design. [Research Report] RR-9175, Inria Bordeaux Sud-Ouest. 2018, pp.1-23. hal-01791072v1

**HAL Id: hal-01791072**

**<https://inria.hal.science/hal-01791072v1>**

Submitted on 14 May 2018 (v1), last revised 12 Sep 2019 (v3)

**HAL** is a multi-disciplinary open access archive for the deposit and dissemination of scientific research documents, whether they are published or not. The documents may come from teaching and research institutions in France or abroad, or from public or private research centers.

L'archive ouverte pluridisciplinaire **HAL**, est destinée au dépôt et à la diffusion de documents scientifiques de niveau recherche, publiés ou non, émanant des établissements d'enseignement et de recherche français ou étrangers, des laboratoires publics ou privés.



# Low-cost non-intrusive sensitivity analysis technique for heat and mass transfer in porous media, with application to space-vehicle heat-shield design

Mickaël Rivier, Jean Lachaud , Pietro Marco Congedo

**RESEARCH  
REPORT**

**N° 9175**

May 14, 2018

Project-Teams CARDAMOM





## Low-cost non-intrusive sensitivity analysis technique for heat and mass transfer in porous media, with application to space-vehicle heat-shield design

Mickaël Rivier<sup>\*†</sup>, Jean Lachaud<sup>‡</sup>, Pietro Marco Congedo<sup>§</sup>

Project-Teams CARDAMOM

Research Report n° 9175 — May 14, 2018 — 23 pages

**Abstract:** A low-cost non intrusive sensitivity analysis technique is applied to heat and mass transfer in porous media. To illustrate the approach, the Analysis of Variance (ANOVA) functional expansion is explicitly derived on an analytic problem - heat transfer in solid materials. Then, a non-intrusive formulation is proposed for heat and mass transfer computer codes. It relies on an Anchored-ANOVA strategy permitting to perform low-cost sensitivity analysis in problems featuring a large number of uncertain parameters. Its applicability to complex heat and mass transfer problems is demonstrated for space vehicle heat-shield design. The sensitivity analysis method has been coded in a computer program that has been interfaced with the Porous material Analysis Toolbox based on OpenFOAM (PATO) released Open Source by NASA. Then, a Polynomial-Chaos method is used in order to compute the statistics of some quantities of interest for the atmospheric entry of the Stardust capsule, by taking into account uncertainties on heat-shield material properties and chemistry models.

**Key-words:** Sensitivity analysis, Uncertainty quantification, Porous media, Heat-shield ablation

---

\* Inria Bordeaux Sud-Ouest - Team CARDAMOM

† ArianeGroup, Le Haillan

‡ C la Vie, University of New Caledonia, New Caledonia

§ DeFI - CMAP - Ecole Polytechnique, Inria Saclay - Ile de France, Polytechnique - X, CNRS

**RESEARCH CENTRE  
BORDEAUX – SUD-OUEST**

351, Cours de la Libération  
Bâtiment A 29  
33405 Talence Cedex

## **Méthode d'analyse de sensibilité non intrusive à faible coût pour les transferts thermique et massique en milieu poreux, appliquée à la conception des boucliers thermiques de véhicules spatiaux**

**Résumé :** Une technique d'analyse de sensibilité non intrusive à faible coût est appliquée au problème de transfert thermique et massique en milieu poreux. Afin d'illustrer l'approche, la formulation fonctionnelle appelée Analysis of Variance (ANOVA) est explicitée sur un problème analytique de transfert thermique. Une formulation non intrusive est ensuite proposée pour se coupler à un code de calcul. Celle-ci repose sur la stratégie Anchored-ANOVA, permettant de réaliser des analyses de sensibilité à faible coût malgré le grand nombre de paramètres incertains des problèmes étudiés. Cette stratégie a été appliquée avec succès dans le cadre de problèmes complexes de transfert thermique et massique visant la conception des boucliers thermiques de véhicules spatiaux. La méthode d'analyse de sensibilité a été implémentée dans un programme interfacé avec l'outil Porous material Analysis Toolbox based on OpenFOAM (PATO), diffusé en Open Source par la NASA. Enfin, la méthode des Polynômes du Chaos est utilisée afin d'obtenir différentes statistiques des quantités d'intérêt lors de l'entrée atmosphérique de la capsule Stardust, en considérant des incertitudes sur les matériaux ainsi que sur les modèles chimiques.

**Mots-clés :** Analyse de sensibilité, Quantification des incertitudes, Milieu poreux, Abalation de bouclier thermique

## 1 Introduction

Heat and mass transfer in porous media is a discipline that finds numerous industrial applications. The discipline may be split in several fundamental investigation areas: heat transfer by conduction [1, 2] and by radiation [3, 4], mass transport by diffusion [5, 2, 6] and by convection [7, 8], heterogenous [9] and homogeneous [10, 11] chemical reactions, morphological evolutions [12]. In some instances, engineering applications require modeling several phenomena in a coupled manner to predict heat and mass transfer with a good accuracy, e.g. heat shields of space vehicles [13, 14, 15], nozzle's walls of rocket thrusters [16, 17], biomass pyrolysis [18, 19], cracking [20, 21, 22], chemical vapor infiltration [23, 24], etc. As proposed in [25, 26], three main steps need be undertaken for computational design : (1) sensitivity analyses on a detailed model, (2) uncertainty quantification, and (3) optimization using an engineering model. Sensitivity analyses are useful to determine the key parameters. The model can sometimes be simplified at this stage and the detailed model is replaced by an engineering model. The key parameter uncertainties are then propagated to obtain the design uncertainties to be used in the margin policy. If within validation range, the model is then used for design, which is an optimization process, be it automatic or a simple try and error process. Ideally, these three steps should be undertaken each time material properties or operating conditions are modified. However, one clear limitation of increasingly complicated models is the computational cost of extensive sensitivity analyses.

The objective of this work is to illustrate the application of an advanced sensitivity analysis technique to a detailed heat and mass transfer models in porous media at a reduced cost. In literature, uncertainty propagation has been already performed alongside Global Sensitivity Analysis for problems of natural convection in [27]. Uncertainty analyses have also been performed on chemical rates and their effect on aeroheating predictions for Mars entry in [28], and on ablation problems in plasma wind tunnel [29, 30]. A recent study concerning the laser ablation of aluminum has been also presented in [31].

Section 2 is devoted to the presentation of the uncertainty quantification techniques used in this paper. First, a sensitivity analysis approach is applied for illustration and verification to an analytical transient heat transfer problem. Then, the Anchored-Anova based strategy is presented. Moreover, some generalities on Polynomial-Chaos method are provided, since it is used to generate a surrogate model on the reduced problem formulated after the first sensitivity analysis. In section three, we present the application of the UQ methods to study the thermal response of the ablative thermal protection system of the NASA Stardust sample-return capsule during its re-entry into the Earth's atmosphere. The heat and mass transfer simulation tool is the Porous material Analysis Toolbox based on OpenFoam (PATO), a NASA software program available open source. Uncertainties on material and chemistry models are propagated on quantities of interest - as ablation rate and internal temperature. Finally, Section 4 draws some conclusions and perspectives.

## 2 Sensitivity and uncertainty analysis theory and tools

Let us consider a stochastic differential equation of the form:

$$L(\mathbf{x}, \boldsymbol{\xi}, \phi) = f(\mathbf{x}, \boldsymbol{\xi}) \quad (1)$$

where  $L$  is a non-linear spatial differential operator (for instance,  $L$  is the steady Navier-Stokes operator) depending on a set of uncertainties, defined with a random vector  $\boldsymbol{\xi}$  (whose dimension depends on the number of uncertain parameters in the problem) and  $f(\mathbf{x}, \boldsymbol{\xi})$  is a source term depending on the position vector  $\mathbf{x}$  and on  $\boldsymbol{\xi}$ . In the following, we drop the dependence on  $\mathbf{x}$

in order to simplify the notation. The solution of the stochastic equation (1) is  $\phi(\boldsymbol{\xi})$ , which is a function of the space variable  $\mathbf{x} \in \mathbb{R}^d$  and of  $\boldsymbol{\xi} \in \Xi = \Xi_1 \times \cdots \times \Xi_N$  ( $\Xi \subset \mathbb{R}^N$ ) and  $\boldsymbol{\xi} \in \Xi \mapsto \phi(\boldsymbol{\xi}) \in L^2(\Xi, p(\boldsymbol{\xi}))$ , where  $p(\boldsymbol{\xi}) = \prod_{i=1}^N p(\xi_i)$  is the probability density function of  $\boldsymbol{\xi}$ .

One of the objective of Uncertainty Quantification is to compute the statistics of the quantity of interest, *i.e.*  $\phi(\boldsymbol{\xi})$ .

We can define the central statistical moment of  $\phi$  of order  $n$  as

$$\mu^n(f) = \int_{\Xi} (\phi(\boldsymbol{\xi}) - E(\phi))^n p(\boldsymbol{\xi}) d\boldsymbol{\xi}, \quad (2)$$

where  $E(\phi)$  indicates the expected value of  $\phi$

$$E(\phi) = \int_{\Xi} \phi(\boldsymbol{\xi}) p(\boldsymbol{\xi}) d\boldsymbol{\xi}. \quad (3)$$

In the following, we indicate with  $\sigma^2$ , the variance (second-order moment). We illustrate the main concepts of the ANOVA-decomposition in Section 2.1. Then, to clearly present the context of uncertainty analysis theory and provide a comprehensive understanding of the approach followed in this work, we will use as illustration a monodimensional heat transfer problem presented in Section 2.2. The UQ methods are then described in Section 2.3.

## 2.1 ANOVA-based decomposition

Let us suppose that the response of a given system of interest can be represented by a  $N$ -dimensional function :

$$y = \phi(\boldsymbol{\xi}) = \phi(\boldsymbol{\xi}_1, \boldsymbol{\xi}_2, \cdots, \boldsymbol{\xi}_N) \quad (4)$$

We consider Eq. (4) in its functional expansion form as follows

$$y = \phi_0 + \sum_{1 \leq i \leq N} \phi_i(\boldsymbol{\xi}_i) + \sum_{1 \leq i < j \leq N} \phi_{ij}(\boldsymbol{\xi}_i, \boldsymbol{\xi}_j) + \cdots + \phi_{1,2,\dots,N}(\boldsymbol{\xi}_1, \boldsymbol{\xi}_2, \cdots, \boldsymbol{\xi}_N)$$

or in compact form using a multi index system:

$$y = \phi_{s_0} + \sum_{j=1}^{2^N-1} \phi_{s_j}(\boldsymbol{\xi}_{s_j}) \quad (5)$$

The multi indices  $s_j$  are defined such as

$$\begin{aligned} s_0 &= (0, 0, 0, \cdots, 0) \\ s_1 &= (1, 0, 0, \cdots, 0) \\ s_2 &= (0, 1, 0, \cdots, 0) \\ &\vdots \\ s_N &= (0, 0, 0, \cdots, 1) \\ s_{N+1} &= (1, 1, 0, \cdots, 0) \\ s_{N+2} &= (1, 0, 1, \cdots, 0) \\ &\vdots \\ s_{\mathcal{N}} &= (1, 1, 1, \cdots, 1) \end{aligned} \quad (6)$$

where  $\mathcal{N} = 2^N - 1$ . The representation of Eq. (5) is called ANOVA (Analysis Of Variance) decomposition [32] of  $\phi(\boldsymbol{\xi})$ , if for any  $j \in \{1, \dots, \mathcal{N}\}$ ,

$$\int_{\mathbb{R}} \phi_{s_j}(\boldsymbol{\xi}_{s_j}) p(\boldsymbol{\xi}_i) d\boldsymbol{\xi}_i = 0 \quad \text{for } \boldsymbol{\xi}_i \in \{\boldsymbol{\xi}_{s_j}\} \quad (7)$$

It follows from Eq. (7) the orthogonality of ANOVA component terms, namely

$$E(\phi_{s_j} \phi_{s_k}) = 0 \quad \text{for } j \neq k \quad (8)$$

ANOVA allows identifying the contribution of a given stochastic parameter to the total variance of an output quantity. Meanwhile, we obviously have

$$E(\phi_{s_j}) = 0 \quad \text{for } j = 1, \dots, \mathcal{N}$$

Note that the terms in the ANOVA decomposition can be expressed as integrals of  $\phi(\boldsymbol{\xi})$ . Indeed, we have

$$\begin{aligned} E(Y) &= \phi_0 \\ E(Y|\boldsymbol{\xi}_i) &= \phi_0 + \phi_i(\boldsymbol{\xi}_i) \\ E(Y|\boldsymbol{\xi}_i, \boldsymbol{\xi}_j) &= \phi_0 + \phi_i(\boldsymbol{\xi}_i) + \phi_j(\boldsymbol{\xi}_j) + \phi_{ij}(\boldsymbol{\xi}_i, \boldsymbol{\xi}_j) \end{aligned} \quad (9)$$

and so on, where  $E(Y|\cdot)$  denotes the conditional expectation.

## 2.2 Analytical solution for transient heat transfer

### 2.2.1 Deterministic problem

Effective heat transfer is the main mode of energy transport in most porous materials. Let us consider a homogeneous semi-infinite unidimensional medium. Under the assumption of constant material properties, the transient heat transfer equation is given by

$$\partial_t T = \alpha \partial_x^2 T \quad (10)$$

where  $\alpha = k/(\rho \times c_p)$  is the diffusivity. We will consider a medium initially at the room temperature  $T(x, t = 0) = T_0 = 300K$ . Its surface temperature is taken to  $T(x = 0, t) = T_w = 1646 K$  at the start of the experiment. Laplace transform is used for its resolution as presented in Appendix A. The temperature profile as a function of time and space is given by

$$T(x, t) = T_0 + (T_w - T_0) \operatorname{erfc} \left( \frac{x}{2\sqrt{\alpha t}} \right) \quad (11)$$

where **erfc** is the complementary error function. The temperature profiles computed for times of 1, 10 and 60 seconds are plotted in Fig. 1 for a representative medium of diffusivity of  $10^{-7} m^2/s$ . We will only consider in the illustrations that follow the first centimeter of the medium. We see here that the hypothesis that the medium is semi-infinite does not play a role on the result, as the heat wave hasn't reached the one centimeter mark after one minute of heating.

### 2.2.2 Formulation under uncertainty

Let us now formulate the problem presented in Eq. 10 under an uncertainty quantification perspective. In particular, let assume that two parameters are affected by some variability and/or are not well-known : a 5% of variation in terms of min/max is then imposed on  $T_w$  and  $\alpha$  considering a uniform distribution (with respect to the deterministic values previously

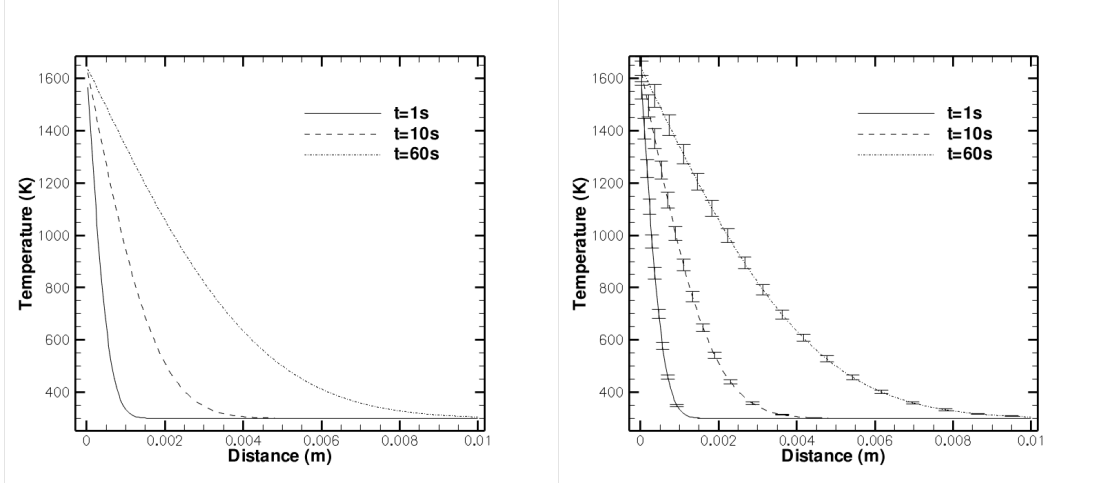


Figure 1: Analytical solution for unidimensional transient heat transfer with fixed surface temperature, for a semi-infinite medium of thermal diffusivity  $10^{-7} \text{ m}^2/\text{s}$ . Initial temperature of the body: 300 K; surface temperature : 1646 K. Left: temperature profiles for 1, 10, and 60 seconds. Right: error bars in terms of standard deviation when considering two uncertainties.

used, denoted in the following as  $T_{wm}$  and  $\alpha_m$ , respectively). The problem is now formulated as follows:

$$\partial_t T = \alpha \partial_x^2 T = \alpha_m \times (0.95 + (1.05 - 0.95) * \xi_2) \partial_x^2 T \quad (12)$$

where  $T_w = T_{wm} \times (0.95 + (1.05 - 0.95) * \xi_1)$ , and  $\xi_1, \xi_2$  vary in  $[0, 1]$ .

Several methods can be used in order to solve the problem defined in Eq. 12. In this work, we use systematically the so-called non-intrusive methods: this means that a single deterministic computation (used to solve for example the differential operator defined in Eq. 10) is replaced with a whole set of such computations, each one of those being run for specific values of the uncertain conditions. The final solution can be then written as follows:

$$T(x, t, \xi_1, \xi_2) = T_0 + (T_{wm}(0.95 + 0.1\xi_1) - T_0) \operatorname{erfc} \left( \frac{x}{2\sqrt{\alpha_m(0.95 + 0.1\xi_2)t}} \right). \quad (13)$$

Now, let us show how the computation of the variance and the computation of the contribution of each source of uncertainty can be reduced only to the computation of some integrals on the analytical solution shown in Eq. 13 for some fixed values of  $x$  and  $t$ :

The ANOVA functional expansion (more details are provided in the next subsection) is a unique tool for assessing the contribution of each uncertainty (and of the interactions) to the global variance. This is computed as follows (variables  $x$  and  $t$  are dropped since this does not change the following developments)

$$T(\xi) = T_0 + T_{\xi_1} + T_{\xi_2} + T_{\xi_1 \xi_2}, \quad (14)$$

where

$$\begin{aligned}
T_0 &= \int_{\Xi^2} T(\boldsymbol{\xi})p(\boldsymbol{\xi})d\boldsymbol{\xi}; \\
T_{\xi_1} &= \int_{\Xi} T(\boldsymbol{\xi})p(\xi_2)d\xi_2 - T_0; \\
T_{\xi_2} &= \int_{\Xi} T(\boldsymbol{\xi})p(\xi_1)d\xi_1 - T_0; \\
T_{\xi_1\xi_2} &= T(\boldsymbol{\xi}) - T_{\xi_1} - T_{\xi_2} - T_0.
\end{aligned} \tag{15}$$

The overall variance  $\sigma^2$  can be computed by means of the ANOVA expansion as

$$\sigma^2 = \sigma_{\xi_1}^2 + \sigma_{\xi_2}^2 + \sigma_{\xi_1\xi_2}^2, \tag{16}$$

where

$$\begin{aligned}
\sigma_{\xi_1}^2 &= \int_{\Xi} T_{\xi_1}^2 p(\xi_1) d\xi_1; \\
\sigma_{\xi_2}^2 &= \int_{\Xi} T_{\xi_2}^2 p(\xi_2) d\xi_2; \\
\sigma_{\xi_1\xi_2}^2 &= \int_{\Xi^2} T_{\xi_1\xi_2}^2 p(\boldsymbol{\xi}) d\boldsymbol{\xi}.
\end{aligned} \tag{17}$$

Note that  $\sigma_{\xi_1}^2$ ,  $\sigma_{\xi_2}^2$  represent the unique contribution of  $\xi_1$  and  $\xi_2$  to the global variance  $\sigma^2$ , respectively. Moreover,  $\sigma_{\xi_1\xi_2}^2$  represents the contribution given by the interaction between  $\xi_1$  and  $\xi_2$ .

Note that only integrals of the expression defined in Eq. 13 are required, in order to compute the contributions to the variance for fixed values of  $(x, t)$ . In Figure 1 (on the right), the solution is then represented in terms of mean and the associated error bars (square root of the variance, *i.e.* standard deviation). Figure 2 illustrates the variance of the temperature at a time of 60s, including the contribution of each uncertainty. Note that the uncertainty on  $T_w$  is predominant and justifies the most part of the global variability of the temperature, with respect to the input uncertainties. Finally, this simple example illustrates the interest in propagating some physical input uncertainties through the numerical model.

### 2.3 Non-intrusive formulations for expensive computer codes

Unfortunately, generally it is not possible to compute an analytical solution of the problem defined in Eq. 1. This could require the resolution of a complex system of equation, producing a numerical approximation of the solution on some discretized grid of the numerical domain. Note then that computing the integrals of Eq. 17 can be very costly. Moreover, some additional issues could come if a large number of uncertainties should be treated, if the quantity of interest feature some discontinuities. The real challenge is then to formulate an efficient numerical algorithm permitting to build an accurate representation of the quantity of interest as a function of input uncertainties.

As previously mentioned, only non-intrusive strategy are targeted in this work. In particular, here, we tackle a problem featuring a large number of uncertainties, that can be very challenging to solve, due to the so-called Curse of Dimensionality. This is associated to a loss of convergence for any method for an increasing number of parameters and then an infeasible number of calculations to perform. For this reason, we have cured this problem with a two-steps approach. In

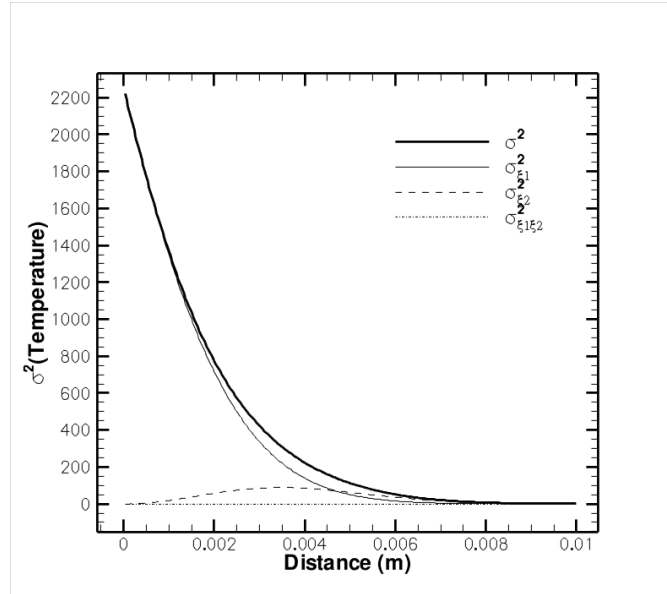


Figure 2: Variance of the temperature (including the contribution of each uncertainty) at a time of 60 seconds.

the first one, we applied an anchored-ANOVA approach for the global problem. This analysis permits to detect the hierarchy of the most predominant uncertainties and sensibly reduced the number of deterministic simulations needed to perform the stochastic analysis. In a second step, we applied a Polynomial-Chaos approach for treating the subspace including only the important parameters, that could provide a good representation of the quantity of interest in the stochastic space.

As mentioned before, due to the non-intrusive character of the stochastic methods considered here, the coupling with PATO, or any other heat and mass transfer computational model, is very straightforward : it reduces to the creation of a small interface for building automatically PATO input parameters files for each set of uncertain conditions.

Both methods are described briefly in the following. For more details, refer to [33] for the Polynomial-based method and to [34] for the anchored-ANOVA approach.

### 2.3.1 Anchored-ANOVA approach: Definitions and basic notions

In order to introduce the less expensive *anchored ANOVA*, the Dirac measure is used in integrations in Eq. (9):

$$p(\xi_i) d\xi_i = \delta(\xi_i - c_i) d\xi_i \quad \text{for } i = 1, \dots, N \quad (18)$$

Thus,  $p(\xi) d\xi = \delta(\xi - \mathbf{c}) d\xi$ . The point  $\mathbf{c} = (c_1, \dots, c_N)$  is called “anchor point”. Hence, the ANOVA component terms in Eq. (9) can be expressed as follows:

$$\begin{aligned} \phi(\mathbf{c}) &= \phi_0 \\ \phi(\mathbf{c}|\xi_i) &= \phi_0 + \phi_i(\xi_i) \\ \phi(\mathbf{c}|\xi_i, \xi_j) &= \phi_0 + \phi_i(\xi_i) + \phi_j(\xi_j) + \phi_{ij}(\xi_i, \xi_j) \\ &\vdots \end{aligned} \quad (19)$$

The formulae in Eq. (19) are used to quantify the expectation and variance of the component functions, by simply evaluating the model outputs at chosen sampling points. For more details, see [34]. This permits a strong reduction of the computational cost, since this avoids the computation of several integrals. Moreover, a variance-based adaptive criterion (see for more details [35]) is used in order to compute the so-called effective dimension and to evaluate high-order interactions with a reduced computational cost. The order at which the ANOVA model is truncated, is called effective dimension, beyond which the difference between the ANOVA model and the truncated expansion in a certain measure is very small. This implies that we will ignore terms in the ANOVA model corresponding to more than those interactions exceeding the fixed threshold.

In this work, a covariance decomposition of the output variance has been considered, as proposed in [34], in order to accurately compute the statistics using the anchored-ANOVA expansion. The covariance decomposition makes the result less sensitive to the choice of the anchor point if a full expansion of the anchored ANOVA is employed.

### 2.3.2 Polynomial-chaos based approach

Under specific conditions, a stochastic process can be expressed as a spectral expansion based on suitable orthogonal polynomials, with weights associated to a particular probability density function. The first study in this field is the Wiener (1938) process. The basic idea is to project the variables of the problem onto a stochastic space spanned by a complete set of orthogonal polynomials  $\Psi$  that are functions of random variables  $\xi$ . For example, the unknown variable  $\phi$  has the following spectral representation:

$$\phi(\xi) = \sum_{i=0}^{\infty} \phi_i \Psi_i(\xi). \quad (20)$$

In practice, the series in Eq. (20) has to be truncated in terms of the polynomial degree  $p_0$ , where the total number of terms of the series  $M$  is determined by:

$$M + 1 = \frac{(N + p_0)!}{N! p_0!}, \quad (21)$$

where  $N$  is the dimensionality of the uncertainty vector  $\xi$ . Each polynomial  $\Psi_i(\xi)$  is a multivariate polynomial form which involve tensorization of 1D polynomial form. The polynomial basis is chosen accordingly to the Wiener-Askey scheme [36] in order to select orthogonal polynomials with respect to the probability density function  $p(\xi)$  of the input. The orthogonality can be advantageously used to compute the coefficients of the expansion in a non-intrusive PC framework

$$\phi_i = \frac{\langle \phi(\xi), \Psi_i(\xi) \rangle}{\langle \Psi_i(\xi), \Psi_i(\xi) \rangle}, \quad \forall i. \quad (22)$$

Several approaches can be used to estimate PC coefficients. The approach used in this study is based on quadrature formula. As a consequence, the solution of a deterministic problem for each quadrature point is required.

For further details, see Congedo *et al.*[33]. In both cases, once the chaos polynomials and the associated  $\phi_i$  coefficients are computed, the expected value and the variance of the stochastic solution  $\phi_i(\xi)$  are obtained from :

$$E_{PC} = \phi_0 \quad (23)$$

$$Var_{PC} = \sum_{i=1}^N \phi_i^2 \langle \Psi_i^2 \rangle \quad (24)$$

Another interesting property of PC expansion is to make easier sensitivity analysis based on the analysis of variance decomposition (ANOVA). It can be easily computed by using some interesting properties of the previous development [37]. Let us recall here that the contribution to the variance of a given random variables with index  $k$ , *i.e.* the first order Sobol's index, can be obtained by:

$$S_k = \frac{\sum_{i \in \alpha} \phi_i^2 \langle \Psi_i^2(\boldsymbol{\xi}) \rangle}{Var_{PC}} \quad (25)$$

where  $\alpha$  represent the set of indexes associated to a given uncertainty  $k$ . For more details, Ref. [37] is strongly recommended.

### 3 Application to space-vehicle heat shield design

Space exploration missions often include entering a planetary atmosphere at hypersonic speed. A high enthalpy hypersonic shock forms around the spacecraft and kinetic energy is progressively dissipated into heat [38]. Heat is transferred to the surface of the spacecraft by radiation and convection. A suitable heat shield is needed to protect the payload. The level of heat flux increases with entry speed and atmospheric density. For fast hypersonic entries, typically faster than  $8 \text{ km/s}$  from earth orbit, ablative materials are used as Thermal Protection Systems (TPS). These materials mitigate the incoming heat through phase changes, chemical reactions, and material removal [39]. A low-density porous carbon/phenolic composite called PICA was used for the Stardust comet-dust sample-return capsule, which reentered the Earth's atmosphere at  $12.7 \text{ km/s}$  [40]. PICA is made of a carbon fiber preform partially impregnated with phenolic resin.

During atmospheric entry, carbon/phenolic materials undergo thermal degradation and ultimately recession captured by the following physico-chemical phenomena (Figure 3). The phenolic polymer thermally decomposes and progressively carbonizes into a low density carbon form, losing mass while releasing pyrolysis gases. The pyrolysis gases percolate and diffuse to the surface through the network of pores. Reactions within the pyrolysis-gas mixture (homogeneous reactions) and between pyrolysis gases and the char take place with possible coking effects (heterogeneous reactions). Mixing and reaction of the pyrolysis gases with boundary layer gases into the pores of the material occur when boundary layer gases penetrate in the material by forced convection or due to fast diffusion at low pressures [15]. At the surface, the material is removed by ablation and the outer surface recedes. Depending on entry conditions, ablation may be caused by heterogeneous chemical reactions (oxidation, nitridation), phase change (sublimation), and possibly mechanical erosion (often called spallation).

A detailed heat and mass transfer model is required to estimate the performance of the porous material and design the thermal protection system. Two important design criteria are the expected level of recession and the maximum back wall temperature. The objective of this section is to show applicability of the method presented in Section 2 for this complex problem.

In subsections 3.1 and 3.2, we present the problem studied and the physical model, respectively. The uncertainty characterization is illustrated in 3.3. The results of the uncertainty quantification analysis are presented in subsection 3.4.

#### 3.1 Presentation of the problem studied

We study the thermal response of the TPS during the whole reentry, from entry interface to cool down. As in the state-of-the-art approach we assume that the problem is locally monodimensional and we study the material response at the stagnation point, which reaches the highest temperature during the reentry. The thickness of the heat shield is two inches [40].



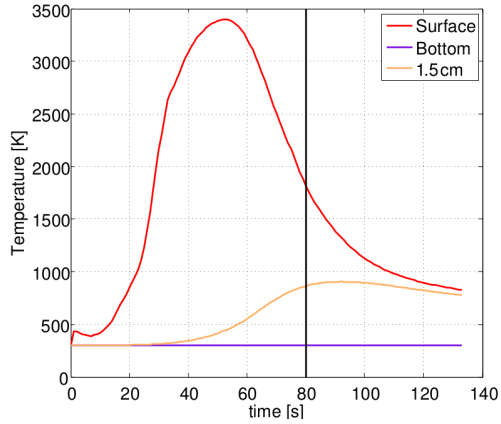


Figure 4: Temperature trend of the reference point at a depth of 1.5 cm inside TACOT material compared to the one of the heated surface, obtained with nominal material parameters.

between the solid phases and the gas phase are modeled at the pore scale assuming local thermal equilibrium. Homogenized models were obtained for solid pyrolysis, pyrolysis species injection in the gas phase, heterogeneous reactions between the solid phases and the gas phase, and homogeneous reactions in the gas phase. The chemistry models were integrated in a macroscopic model making use of volume-averaged governing equations for the conservation of solid mass, gas mass, species (finite-rate chemistry) or elements (equilibrium chemistry), momentum, and energy. The model is implemented in the Porous material Analysis Toolbox (PATO), distributed Open Source by NASA. First-order implicit finite-volume schemes in time and space [44, 45], which have been shown to provide excellent convergence and accuracy [11, 15], were used for the simulations presented in Section 3.4.

As mentioned in the previous section, due to the non-intrusive character of the stochastic methods considered, the coupling with PATO reduces to an interface for building automatically input parameters files for each set of uncertain conditions. Therefore, what follows in the presentation could be done with any other relevant heat and mass transfer simulation tool.

### 3.3 Uncertain parameters and associated uncertainties

In a previous study, uncertain material property parameters have been identified by Mahzari et al. [46] and their uncertainties were propagated using a Monte Carlo technique. We decided to include in our study these uncertain parameters. We also added a set of new parameters to assess the effect of the pyrolysis gas composition on the material response. Indeed, recent publications that occurred after the study of Mahzari have shown that the pyrolysis gas composition strongly varies with time. The pyrolysis gases are composed of carbon, oxygen and hydrogen elements. The pyrolysis gas composition influences the pyrolysis gas enthalpy - which impacts heat transfer in the porous material - and the boundary layer chemistry - which controls the ablation rates and the surface temperature. For this first analysis we allowed an uncertainty of 10% on these elements. The composition in term of species is then computed in each cell of the mesh and at each time step using an equilibrium chemistry solver [15]. This makes the computation very costly and justifies the use of the low-cost method proposed in this study.

In summary, we have used twenty-seven uncertain parameters in the TACOT material model.

We have attributed 5 to 10 % uncertainty to each of them as follows (the number in brackets is the label used to identify each uncertainty in the following of this paper) :

- Density (1) and volume fraction (2) of the fibrous preform (5% uncertainty),
- Density (3) and volume fraction (4) of the phenolic matrix (5% uncertainty),
- Virgin's (5) and char's (6) permeability (5% uncertainty),
- Pyrolysis model (10% uncertainty):
  - Elementary composition of the pyrolysis gases in Carbon (7) , Hydrogen (8) and Oxygen (9),
  - Pyrolysis reaction 1 : pre-exponential factor (10), activation energy (11), pyrolysis enthalpy (12),
  - Pyrolysis reaction 2 : pre-exponential factor (13), activation energy (14), pyrolysis enthalpy (15),
- Thermal properties of virgin material (5% uncertainty): heat capacity (16), orthogonal conductivity (17), radial conductivities (18, 19), emissivity (20), reflectivity (21),
- Thermal properties of charred material (5% uncertainty): heat capacity (22), orthogonal conductivity (23), radial conductivities (24, 25), emissivity (26), reflectivity (27).

### 3.4 Results

The Anchored-ANOVA method is applied to the problem presented in the previous section. We present first the convergence analysis with respect to the global number of samples to consider for getting the statistics of all the quantities of interest well converged. In Anchored-ANOVA, the first-order analysis is based on a chosen number of points per direction. We have reported in Table 1 the outcome of this analysis for the temperature computed at a depth of 1.5cm at a time equal to 80s, in terms of decreasing contributions to the variance, for eight and sixteen points along each direction, respectively (which makes a total number of runs of the solver of 216 and 432, respectively). As it can be observed, errors are quite small, resulting in converged quantity with only eight points per direction. Same conclusions can be drawn for all the other quantities of interest considered in this work, *i.e.* temperatures at different depths, the virgin front and the char front. Results shown in the following rely then on this analysis.

Let us now analyse the results from a quantitative and qualitative point of view. Figure 5 presents the transformation of the ablative material with error bars, which represent the spreading of the quantities of interest in terms of standard deviation. The plotted results are the surface recession - due to ablation - and the propagation of the pyrolysis front. The char 2% and virgin 98% are used in the ablation community to identify almost completely charred material (2% left of virgin matrix) and almost pristine virgin material (98% left of virgin matrix). The charring zone is considered to be between these two accepted limits [41]. Note that, since the heating is quite soft at the beginning of the simulation, the material is fully pyrolysed before being ablated. This explains why the char 2% and the wall curves are clearly separated in this case. The observed variability is very small for the three curves. In fact, for the virgin 98%, which is the worst case, the Coefficient of Variation (standard deviation to mean ratio) is of the order of 3%.

A physical analysis of the results is now presented in terms of the contribution of each uncertainty to several quantities, namely the recession, the virgin front, the char front and the

Table 1: Contribution to the variance of each uncertainty and error analysis with respect to the number of points per direction.

Unc.	Contrib. q16 (%)	Contrib. q8 (%)	$\Delta_{abs}$	$\Delta_{rel}$
24	16.9	16.9	0.0	0.0
3	14.8	14.8	0.0	0.0
4	14.7	14.8	0.1	$6.8 \cdot 10^{-3}$
26	9.03	9.01	0.02	$2.2 \cdot 10^{-3}$
1	8.31	8.32	0.01	$1.2 \cdot 10^{-3}$
2	8.29	8.3	0.01	$1.2 \cdot 10^{-3}$
9	7.63	7.64	0.01	$1.3 \cdot 10^{-3}$
11	5.13	5.13	0.0	0.0
22	4.05	4.05	0.0	0.0
8	2.88	2.88	0.0	0.0
14	2.88	2.88	0.0	0.0
12	2.48	2.48	0.0	0.0
15	1.48	1.48	0.0	0.0
7	1.15	1.15	0.0	0.0
16	0.166	0.166	0.0	0.0
18	$5.05 \cdot 10^{-2}$	$5.03 \cdot 10^{-2}$	$0.2 \cdot 10^{-3}$	$4.0 \cdot 10^{-3}$
10	$3.78 \cdot 10^{-2}$	$3.78 \cdot 10^{-2}$	0.0	0.0
13	$5.81 \cdot 10^{-3}$	$5.81 \cdot 10^{-3}$	0.0	0.0
20	$6.68 \cdot 10^{-4}$	$6.7 \cdot 10^{-4}$	$0.2 \cdot 10^{-5}$	$3.0 \cdot 10^{-3}$
6	$7.22 \cdot 10^{-5}$	$7.21 \cdot 10^{-5}$	$0.1 \cdot 10^{-6}$	$1.4 \cdot 10^{-3}$
5	$1.01 \cdot 10^{-5}$	$1.04 \cdot 10^{-5}$	$0.3 \cdot 10^{-6}$	$3.0 \cdot 10^{-2}$
17	0.0	0.0	0.0	0.0
19	0.0	0.0	0.0	0.0
21	0.0	0.0	0.0	0.0
23	0.0	0.0	0.0	0.0
25	0.0	0.0	0.0	0.0
27	0.0	0.0	0.0	0.0

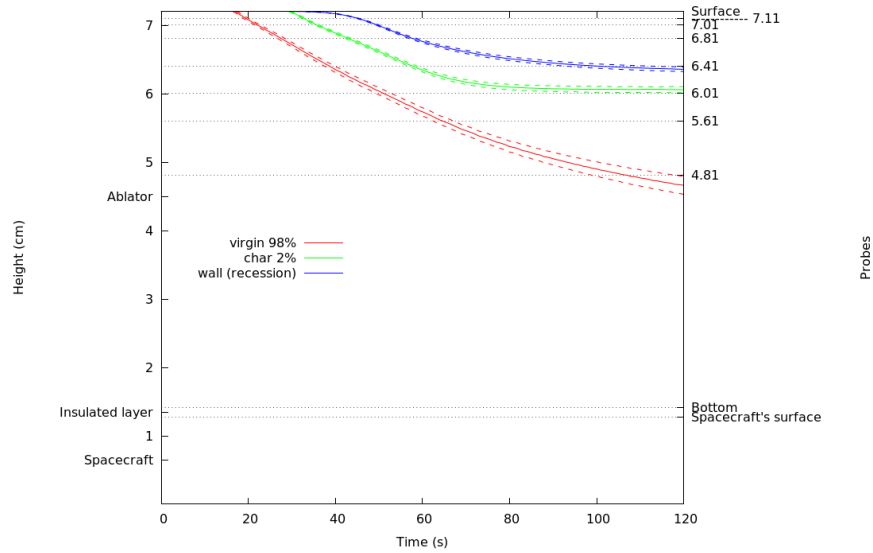


Figure 5: Recession, char at 2% and virgin at 98% with error bars, corresponding to the standard deviation.

surface temperature, as a function of time. The results are presented in Figure 6. They are in qualitative agreements with the findings of Mazhari et al. and in agreement with one would

expect from a dimensionless analysis of the equations. Concerning the recession and the location of the Char 2%, the maximal standard deviation is of the order of 0.03-0.04 cm. As it can be observed in Figure 6b, the behavior of the variance of the location of char 2% is a bit more complex, since it takes into account the parameters influencing the heat transfer in the charred material and the pyrolysis parameters. The virgin 98% is influenced mostly by the uncertainty on the Activation energy 1, which controls the moment when the pyrolysis starts. The surface temperature is mostly driven by the char's emissivity except at the beginning of the pyrolysis reaction, where the activation energies are predominant.

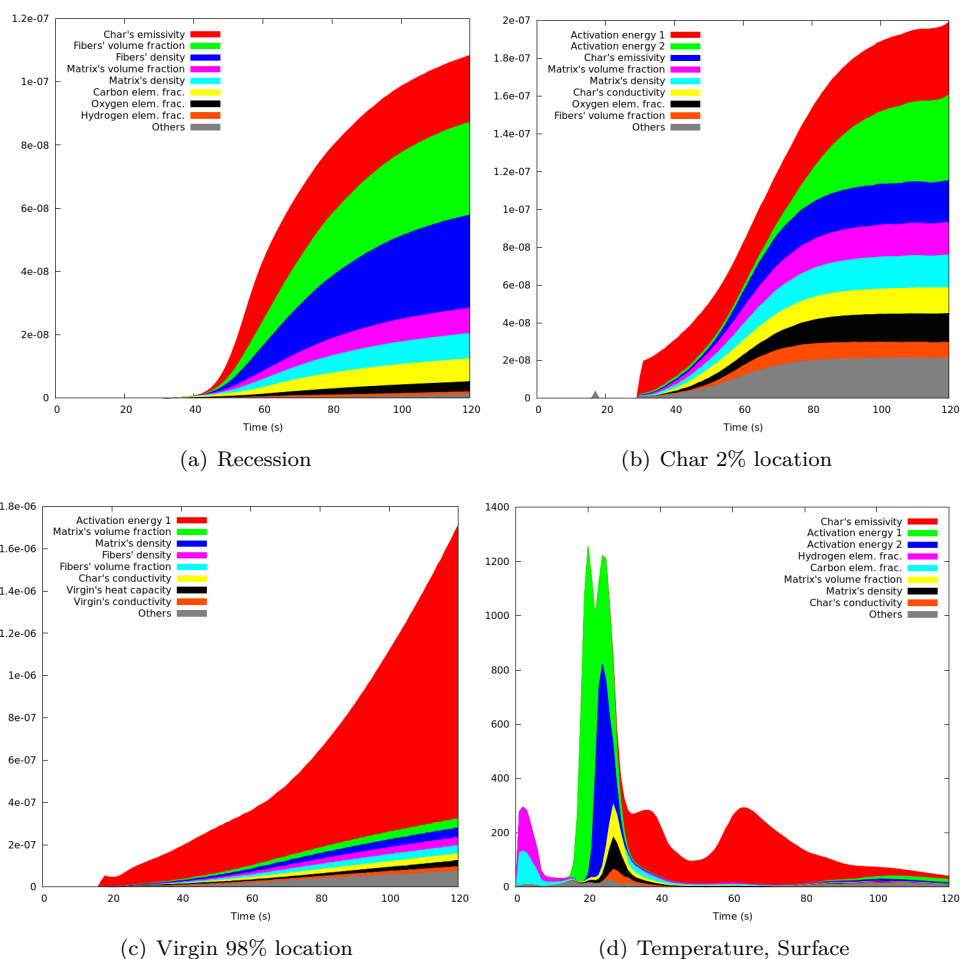


Figure 6: Contributions of each uncertainty to the variance times the variance, computed for several quantities, as a function of time. Units of measure : a)  $[m^2]$  vs  $[s]$ , b)  $[m^2]$  vs  $[s]$ , c)  $[m^2]$  vs  $[s]$ , d)  $[K^2]$  vs  $[s]$ .

We would like to point out a new result. The uncertain parameters introduced in this study (activation energies and pyrolysis gas compositions) clearly propagate uncertainties on the studied quantities. The effect of these uncertainties is observed on the in-depth temperature evolution as well, as shown in Figure 7, where the contributions of each uncertainty to the variance of the temperature is computed over the time at different depths in the material. The

standard deviation of the temperature takes the highest value at a depth of 0.7cm (100 K), while it becomes quite small for the other depths considered here.

With the advancement of the ablation front, first contributions of virgin's parameters and then char's ones' drop. Parameters of pyrolysis and material composition also show decreasing contributions as the pyrolysis reaction comes to an end.

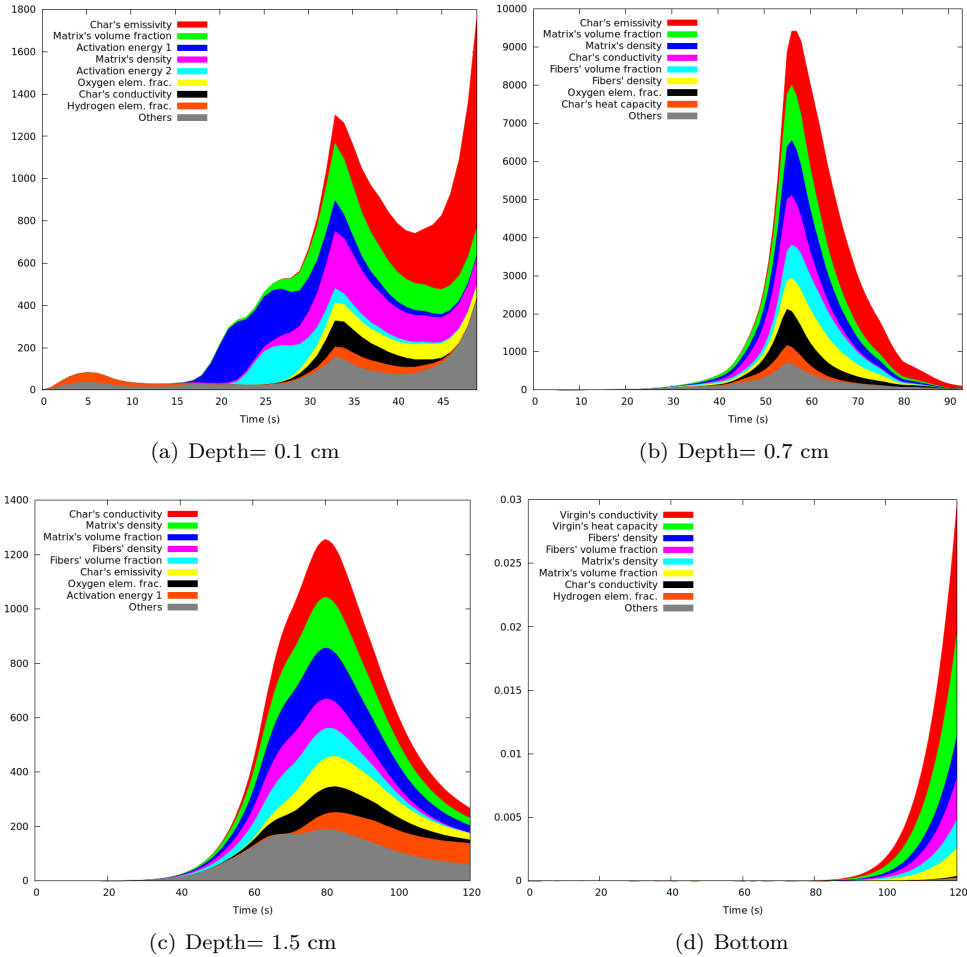


Figure 7: Contributions of each uncertainty to the variance of temperature times the variance, at different depths. Units of measure :  $[K^2]$  vs  $[s]$ .

In order to make more evident the different contributions, Figure 8 illustrates the different contributions gathered in terms of different groups of uncertainty, *i.e.* fibers and matrices properties, TACOT's composition, pyrolysis parameters, etc.

By using the low-cost sensitivity analysis technique, the hierarchy of the most important uncertain parameters contributing to the variance of the temperature can be computed as a function of the depths at a fixed time. For example, in Figure 9 we show the hierarchy at a time of 80 s of entry simulation. As it can be observed, the trend is highly non linear, and this could be particularly useful to build reliable design margin policies and to guide material model development efforts.

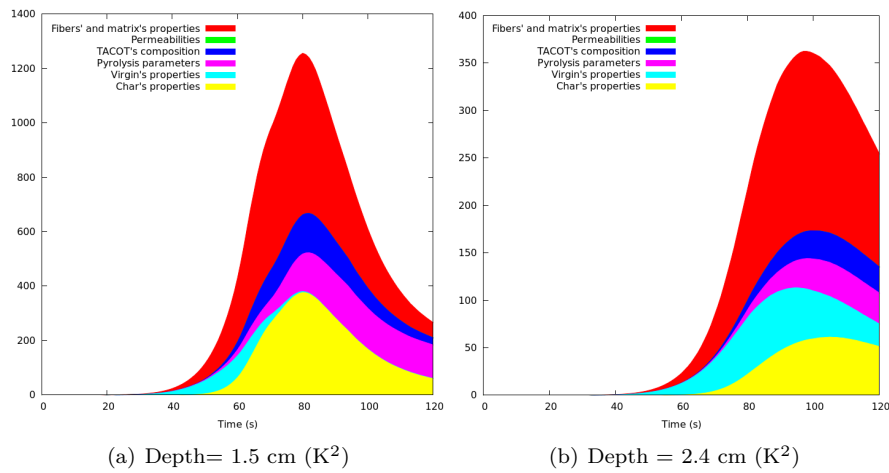


Figure 8: Contributions of each uncertainty to the variance of the temperature times the variance, at different depths, where uncertainties are classified with respect to different groups.

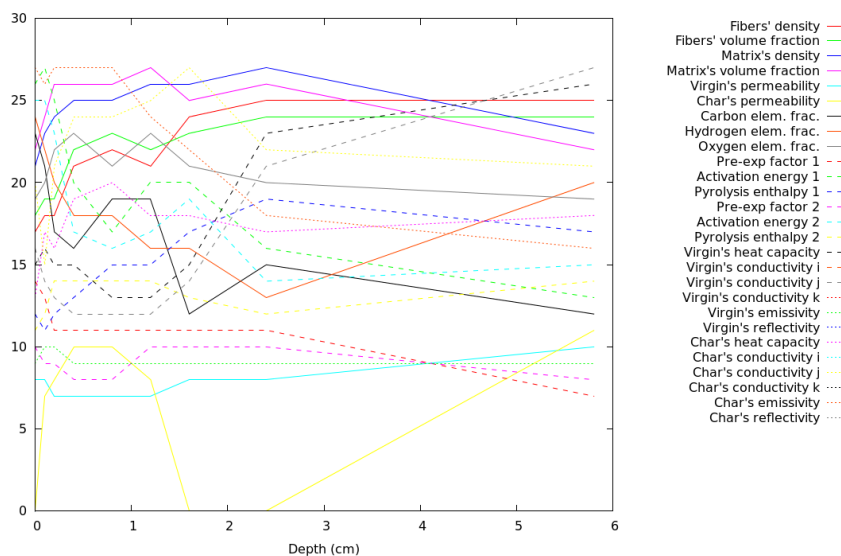


Figure 9: Hierarchy of the uncertain parameters (in terms of Sobol indices (%)) as a function of depth at  $t=80$  s.

### 3.5 Construction of the Polynomial-Chaos based surrogate

As explained in Section 2.3.2, the interest of low-cost sensitivity analysis technique is twofold. More than only identifying a ranking of main uncertainties, it can be used in order to build a surrogate model (a Polynomial-Chaos based one in this case) on a reduced set of uncertainties, *i.e.* the predominant ones. This is applied here to the temperature computed at a depth of 1.5cm for different times. Note that this can be easily applied to a whatever quantity of interest, but the surrogate will be not the same since the most important uncertainties can be different

with respect to the time, the depth and the quantity of interest.

In the case under consideration, first the uncertainties contributing the most to the variance of the temperature at different times are computed (Figure 10 illustrates the ranking for a time  $t = 80s$ ).

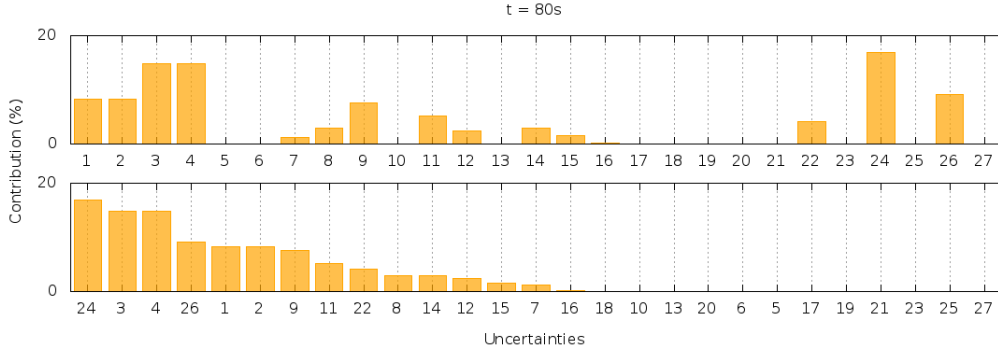


Figure 10: Sorted contributions at a depth of  $1.5cm$  and at a time of  $t = 80s$

Secondly, the PC-based surrogate is constructed on a set of input parameters defined by the predominant uncertainties. For example, at a time  $t = 80s$ , uncertainties labelled as 24, 3, 4, 26, 1, 2, 9, 11 and 22 are chosen as input parameters (See Section 3.3 for identifying each uncertainty).

Obviously, the reduction of the problem yields a loss of accuracy with respect to the statistics computation, which could be estimated. Variance reduction is around 11%, which is mainly due to the high number of significant parameters, which are neglected in the reduced problem.

Using the surrogate model, a whatever post-processing statistical analysis can be done for free. As an example, the Probability Density Function (PDF) of the temperature at different times are computed and represented in Figure 11. As it can be observed, gaussian-like PDF can be observed.

One can see here a very reliable way to design a thermal shield under uncertainties. This study, as a first overview of uncertainty quantification possibilities, heads toward future works, deepening even more the design capabilities of those tools to enhance the concrete results which may be obtained.

## 4 Conclusion

A low-cost sensitivity analysis technique based on ANOVA has been proposed to study complicated heat and mass transfer problems. To clearly explicit the method in the field of material analysis, analytical derivations of the ANOVA method are presented in the case of a well known deterministic heat transfer problem - transient conduction in a solid. Then, a sensitivity analysis technique based on anchored-ANOVA is presented, permitting to treat problems described by expensive computed codes with several uncertainties. This technique has been coupled with PATO, a reactive porous material analysis code distributed Open Source by NASA (<https://software.nasa.gov/software/ARC-16680-1A>, retrieve 8/11/2017). The heat and mass transfer problem occurring in the heat-shield of a space vehicle entering an atmosphere has been studied. The suite of tools have been shown to be efficient to propagate uncertainties and to provide parameter hierarchies in the case of very complicated simulations. Perspectives of this work

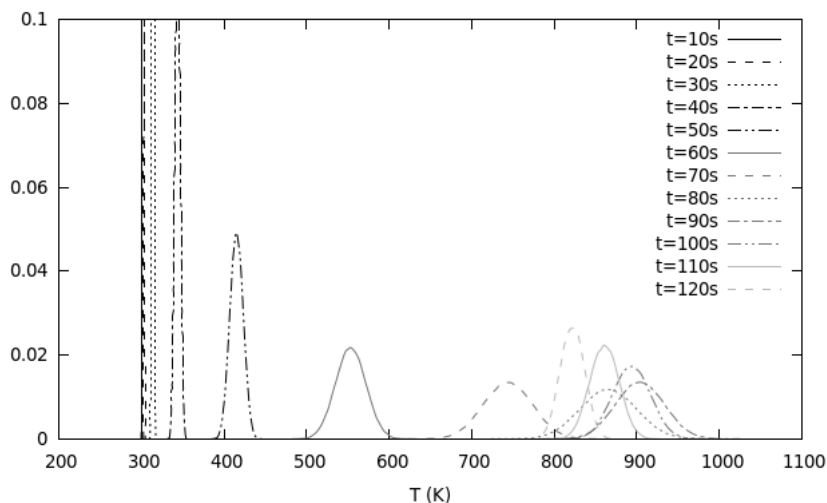


Figure 11: PDF of the temperature at a depth of 1.5cm at different times.

consist in using the suite of tool for inverse problems, e.g. use optimization under uncertainties to optimize material properties for targeted conditions.

## References

- [1] M. Quintard, S. Whitaker, Local thermal equilibrium for transient heat conduction : theory and comparison with numerical experiments, *International Journal of Heat and Mass Transfer* 38 (15) (1995) 2779–2796.
- [2] S. Whitaker, *The method of volume averaging*, Kluwer Academic Publisher, Dordrecht, The Netherlands, 1999.
- [3] M. F. Modest, *Radiative Heat Transfer*, 2nd Edition, McGraw-Hill, New York, 1993.
- [4] J. Taine, F. Enguehard, Characterization of the radiative properties of homogeneous, anisotropic or non homogeneous porous media, in: O. Chazot, F. Panerai (Eds.), *Porous media interaction with high temperature and high speed flows*, NATO, Science and Technology Organization, STO-AVT-261, Paris, France, 2015, p. 22.
- [5] E. A. Mason, A. P. Malinauskas, *Gas transport in porous media: the dusty-gas model*, Chemical engineering monographs, Elsevier, Amsterdam, 1983.
- [6] G. L. Vignoles, Multicomponent diffusion in porous media, in: O. Chazot, F. Panerai (Eds.), *Porous media interaction with high temperature and high speed flows*, NATO, Science and Technology Organization, STO-AVT-261, Paris, France, 2015, p. 22.
- [7] S. Whitaker, *Flow in porous media I: A theoretical derivation of Darcy’s law*, *Transport in Porous Media* 1 (1986) 3–25.
- [8] D. A. Nield, A. Bejan, *Convection in Porous Media*, 3rd Edition, Springer, New-York, 2006.

- [9] J. Guo, M. Quintard, F. Laouafa, Dispersion in porous media with heterogenous reactions, *Transport in Porous Media* 109 (2015) 541–570.
- [10] N. Gascoin, High temperature and pressure reactive flows through porous media, *International Journal of Multiphase Flow* 37 (1) (2010) 24–35, doi:10.1016/j.ijmultiphaseflow.2010.09.001.
- [11] J. Lachaud, N. N. Mansour, Porous material analysis toolbox based on openfoam and applications, *Journal of Thermophysics and Heat Transfer* 28 (2) (2014) 191–202, doi: 10.2514/1.T4262.
- [12] J. Lachaud, I. Cozmuta, N. N. Mansour, Multiscale approach to ablation modeling of phenolic impregnated carbon ablators, *Journal of Spacecraft and Rockets* 47 (6) (2010) 910–921, doi: 10.2514/1.42681.
- [13] R. M. Kendall, E. P. Bartlett, R. A. Rindal, C. B. Moyer, An analysis of the coupled chemically reacting boundary layer and charring ablator: Part I, NASA CR 1060 (1968) 1–96.
- [14] N. Puiroux, M. Prat, M. Quintard, Non-equilibrium theories for macroscale heat transfer: ablative composite layer system, *International Journal of Thermal Sciences* 43 (6) (2004) 541–554.
- [15] J. Lachaud, T. van Eekelen, J. B. Scoggins, T. E. Magin, N. N. Mansour, Detailed chemical equilibrium model for porous ablative materials, *International Journal of Heat and Mass Transfer* 90 (2015) 1034–1045, doi:10.1016/j.ijheatmasstransfer.2015.05.106.
- [16] R. A. Rindal, K. J. Clark, C. B. Moyer, D. T. Flood, Experimental and theoretical analysis of ablative material response in liquid-propellant rocket engine, NASA CR 72301 (1967) 1–230.
- [17] V. Borie, J. Brulard, G. Lengellé, An areothermochemical analysis of carbon-carbon nozzle regression in solid-propellant rocket motors, *Journal of Propulsion and Power* 5 (6) (1989) 665–673.
- [18] C. D. Blasi, Modeling chemical and physical processes of wood and biomass pyrolysis, *Progress in Energy and Combustion Science* 34 (2008) 47–90, doi:10.1016/j.pecs.2006.12.001.
- [19] J. Ratte, F. Marias, J. Vaxelaire, P. Bernada, Mathematical modelling of slow pyrolysis of a particle of treated wood waste, *Journal of Hazardous Materials* 170 (1) (2009) 1023–1040.
- [20] G. F. Sykes, Thermal cracking of phenolic-nylon pyrolysis products on passing through a heated char, NASA TN D-5804 (1967) 1–19.
- [21] G. Fau, N. Gascoin, P. Gillard, M. Bouchez, J. Steelant, Fuel pyrolysis through porous media: Coke formation and coupled effect on permeability, *Journal of Analytical and Applied Pyrolysis* 95 (2012) 180–188.
- [22] L. Romagnosi, N. Gascoin, E. El-Tabach, I. Fedioun, M. Bouchez, J. Steelant, Pyrolysis in porous media: Part 1. numerical model and parametric study, *Energy Conversion and Management* 68 (1) (2013) 63–67.
- [23] G. L. Vignoles, F. Langlais, C. Descamp, A. Mouchon, A. Mouchon, H. L. Poche, N. Reuge, N. Bertrand, CVD and CVI of pyrocarbon from various precursors, *Surface and Coatings Technology* 188–189 (2004) 241–249.

- 
- [24] G. Vignoles, J. Goyh n che, P. Sebastian, J. R. Puiggali, J. Lines, J. Lachaud, P. Delhaes, M. Trinqucostes, The film-boiling densification process for C/C composite fabrication: from local scale to optimization, *Chemical Engineering Science* 61 (17) (2006) 5636–5653.
- [25] M. J. Wright, R. Beck, K. Edquist, D. Driver, S. Sepka, E. Slimko, W. Willcockson, Sizing and margins assessment of the mars science laboratory aeroshell thermal protection system, *Journal of Spacecraft and Rockets* 51 (4) (2014) 1125–1138.
- [26] M. J. Wright, M. Hughes, A. Calomino, M. B. Barnhardt, An overview of technology investments in the NASA entry systems modeling project, *AIAA paper* 1892 (2015) 1–40.
- [27] N. Fajraoui, M. Fahs, A. Younes, B. Sudret, Analyzing natural convection in porous enclosure with polynomial chaos expansions: Effect of thermal dispersion, anisotropic permeability and heterogeneity, *International Journal of Heat and Mass Transfer* 115 (2017) 205 – 224.
- [28] X. Wang, C. Yan, S. Ju, Y. Zheng, J. Yu, Uncertainty analysis of laminar and turbulent aeroheating predictions for mars entry, *International Journal of Heat and Mass Transfer* 112 (2017) 533 – 543.
- [29] A. Turchi, P. M. Congedo, T. E. Magin, Thermochemical ablation modeling forward uncertainty analysis—part i: Numerical methods and effect of model parameters, *International Journal of Thermal Sciences* 118 (2017) 497 – 509.
- [30] A. Turchi, P. M. Congedo, B. Helber, T. E. Magin, Thermochemical ablation modeling forward uncertainty analysis—part ii: Application to plasma wind-tunnel testing, *International Journal of Thermal Sciences* 118 (2017) 510 – 517.
- [31] Y. Wang, G. K. Befekadu, H. Ding, D. W. Hahn, Uncertainty quantification for modeling pulsed laser ablation of aluminum considering uncertainty in the temperature-dependent absorption coefficient, *International Journal of Heat and Mass Transfer* 120 (2018) 515 – 522.
- [32] G. E. B. Archer, A. Saltelli, I. M. Sobol’, Sensitivity measures, anova-like techniques and the use of bootstrap, *Journal of Statistical Computation and Simulation* 58 (1997) 99–120.
- [33] P. M. Congedo, C. Corre, J.-M. Martinez, Shape optimization of an airfoil in a bzt flow with multiple-source uncertainties, *Computer Methods in Applied Mechanics and Engineering* 200 (1) (2011) 216–232.
- [34] K. Tang, P. M. Congedo, R. Abgrall, Sensitivity analysis using anchored anova expansion and high-order moments computation, *International Journal for Numerical Methods in Engineering* 102 (9) (2015) 1554–1584.
- [35] X. Yang, M. Choi, G. Lin, G. Karniadakis, Adaptive {ANOVA} decomposition of stochastic incompressible and compressible flows, *Journal of Computational Physics* 231 (4) (2012) 1587 – 1614.
- [36] D. Xiu, G. E. Karniadakis, The Wiener–Askey Polynomial Chaos for Stochastic Differential Equations, *SIAM Journal on Scientific Computing* 24 (2) (2002) 619–644.
- [37] T. Crestaux, O. P. Le Ma tre, J. M. Martinez, Polynomial chaos expansion for sensitivity analysis, *Reliability engineering and system safety* 94 (7) (2009) 1161 – 1172.

- [38] J. D. Anderson, Hypersonic and high temperature gas dynamics, Mac Graw-Hill, New-York, 1989.
- [39] G. Duffa, Ablative Thermal Protection Systems Modeling, AIAA Education Series, 2013. doi:10.2514/4.101717.
- [40] M. Stackpoole, S. Sepka, I. Cozmuta, D. Kontinos, Post-flight evaluation of stardust sample return capsule forebody heatshield material, AIAA paper 1202 (2008) 1–7.
- [41] J. Lachaud, A. Martin, T. van Eekelen, I. Cozmuta, Ablation test-case series #2, version 2.8, Jan. 2011, 8 p., prepared for the 5th Ablation Workshop, Feb. 28-March. 1, Lexington, Kentucky.
- [42] K. A. Trumble, I. Cozmuta, S. Sepka, P. Jenniskens, Post-flight aerothermal analysis of the stardust sample return capsule, AIAA paper 1201 (2008) 1–15.
- [43] J. Lachaud, J. B. Scoggins, T. E. Magin, M. G. Meyer, N. N. Mansour, A generic local thermal equilibrium model for porous reactive materials submitted to high temperatures, International Journal of Heat and Mass Transfer 108 (2017) 1406–1417.
- [44] H. Jasak, Error analysis and estimation for the finite volume method with applications to fluid flows, Ph.D. thesis, Imperial College London (University of London) (1996).
- [45] H. G. Weller, G. Tabor, H. Jasak, C. Fureby, A tensorial approach to computational continuum mechanics using object-oriented techniques, Computers in physics 12 (6) (1998) 620–631.
- [46] M. Mahzari, I. Cozmuta, I. Clark, R. Braun, An inverse parameter estimation methodology for the analysis of aeroheating and thermal protection system experimental data, AIAA paper 4027.

## Appendix A

Detailed demonstrations of the analytical resolution of the transient heat transfer equation given by

$$\partial_t T - \alpha \partial_x^2 T = 0, \quad (26)$$

where  $\alpha$  is a constant diffusivity, appears to be hard to find in text books. We will present its resolution using the Laplace transform for a semi-infinite unidimensional medium, with the following boundary conditions

- $T(\forall x, t < 0) = T_0$
- $T(x = 0, t \geq 0) = T_w$

corresponding to a homogeneous medium for which the surface temperature is suddenly raised. Let us apply a variable change that will simplify the integration :  $\theta(x, t) = T(x, t) - T_0$ . Applying the change of variable and the Laplace transform, Eq. 26 rewrites

$$\int_0^\infty e^{-st} \partial_x^2 \theta dt - \frac{1}{\alpha} \int_0^\infty e^{-st} \partial_t \theta dt = 0 \quad (27)$$

In the Laplace space, the variable is defined as  $\theta^* = \int_0^\infty e^{-st} \theta dt$ . After permutation (between  $\int_0^\infty \cdot$  and  $\partial_x^2 \cdot$ ) and integration of the first integral, we obtain

$$\partial_x^2 \theta^*(x) - \frac{1}{\alpha} [s \theta^*(x) - \theta(x, 0)] = 0 \quad (28)$$

Thanks to the change of variable, we have  $\theta(x, 0) = 0$  and Eq. 28 simplifies into

$$\partial_x^2 \theta^*(x) - \frac{s}{\alpha} \theta^*(x) = 0 \quad (29)$$

The solution of this second order ordinary differential equation is

$$\theta^*(x) = A \exp(\sqrt{s/\alpha} x) + B \exp(-\sqrt{s/\alpha} x) \quad (30)$$

where A and B are determined with the boundary conditions. On the semi-infinite domain, we have

- $A = 0$  as the temperature has to have a limit when x tends towards infinity.
- $\theta^*(x = 0) = B$ . From  $\theta(0, t) = T_w - T_0$ , one obtains  $B = (T_w - T_0)/s$  after applying Laplace transform.

Hence, we have

$$\theta^*(x) = \frac{T_w - T_0}{s} \exp(-\sqrt{s/\alpha} x) \quad (31)$$

Returning to the temporal space is done using the space change relation:  $\exp(-a\sqrt{s})/s \Leftrightarrow 1 - \text{erf}(a/(2\sqrt{t}))$ , where *erf* is the error function. After some algebra and returning to variable  $T$ , we obtain the physical temperature profile as a function of time

$$T(x, t) = T_0 + (T_w - T_0) \left[ 1 - \text{erf} \left( \frac{x/\sqrt{\alpha}}{2\sqrt{t}} \right) \right] \quad (32)$$



**RESEARCH CENTRE  
BORDEAUX – SUD-OUEST**

351, Cours de la Libération  
Bâtiment A 29  
33405 Talence Cedex

Publisher  
Inria  
Domaine de Voluceau - Rocquencourt  
BP 105 - 78153 Le Chesnay Cedex  
[inria.fr](http://inria.fr)

ISSN 0249-6399